Remote Sensing of Environment 201 (2017) 243–255

Contents lists available at ScienceDirect

Remote Sensing of Environment

journal homepage: www.elsevier.com/locate/rse

Separate segmentation of multi-temporal high-resolution remote sensing images for object-based change detection in urban area

Xueliang Zhang, Pengfeng Xiao*, Xuezhi Feng, Min Yuan

Department of Geographic Information Science, School of Geographic and Oceanographic Sciences, Nanjing University, Nanjing 210023, China
Collaborative Innovation Center of South China Sea Studies, Nanjing 210023, China
Jiangsu Center for Collaborative Innovation in Geographical Information Resource Development and Application, Nanjing 210023, China

ARTICLE INFO

Keywords:
High-resolution remote sensing
Object-based change detection
Multi-temporal segmentation
Spatial correspondence
Object-to-object change

ABSTRACT

High-resolution (HR) remote sensing images present geometric details of land surface. Object-based change detection (OBCD) provides an effective solution to reveal detailed changes of geographic objects in HR images. In OBCD, the separate segmentation strategy holds the potential of revealing specific object-to-object changes, but it is difficult to establish spatial correspondence between distinct multi-temporal segments. To overcome this difficulty, we proposed to first detect multi-temporal changed objects based on separate segmentations and then to establish spatial correspondence between changed objects at different phases. Three separate segmentation strategies, named as SIISeg, SAISeg, and SAOSeg, are compared to indicate the importance of associating separate segmentation procedures for successive spatial correspondence establishment. The experiments of detecting building changes in urban area are performed to demonstrate the success, benefits, and potentials of establishing spatial correspondence for object-to-object change detection.

1. Introduction

High-resolution (HR) remote sensing images provide a great amount of details of land surface, allowing detailed comparison of geographic objects at different phases. Detecting detailed changes of geographic objects is of great significance to map updating, urban planning and management, disaster management, and so on (Gong et al., 2008; Linke et al., 2009).

Since the geometric details of geographic objects are clearly presented, both thematic and geometric changes of geographic objects can be revealed from multi-temporal HR images, where the geometric changes involve the change of size, shape, position, number, and so on (Blaschke, 2005). Taking the buildings in urban area as an example (Fig. 1), different kinds of building changes, including the new, dismantled, and restored buildings, are presented with object-to-object geometric change in addition to thematic change. A single change map is able to describe the changed regions and the thematic changes in these regions. However, it cannot reveal the object-to-object geometric changes, which is important for understanding the changing process of geographic objects. The focus of this study is to achieve object-to-object change detection by comparing separate segmentations of multi-temporal HR images.

To detect changes of geographic objects from HR images, the object-based change detection (OBCD) has been demonstrated to be an effective method because: (1) image objects can delineate geographic entities better than pixels; and (2) OBCD can exploit abundant features of image objects for comparison (Blaschke et al., 2014; Chen et al., 2012; Hussain et al., 2013; Tewkesbury et al., 2015). Furthermore, OBCD shows a lower sensitivity to misregistration errors than pixel-based change detection (Chen et al., 2014; Dingle Robertson and King, 2011). Generally, OBCD is composed of image segmentation to generate image objects and successive change analysis on image objects to detect changed objects. The effectiveness of OBCD is highly dependent on the segmentation step by providing the same unit or different units for successive change analysis.

Providing the same unit means producing a single segmentation result from multi-temporal images. The solutions include: (1) only segmenting one image and directly assigning the segments to the other image (Comber et al., 2004); (2) stacking images at different phases and segmenting the stacked image (Bontemps et al., 2008, 2012; Conchedda et al., 2008; Desclée et al., 2006; Duveiller et al., 2008; Im et al., 2008; Park and Chi, 2008; Stow et al., 2008; Zhou et al., 2015); (3) separately segmenting images at different phases and fusing the segmentation results into one map by spatial intersection operation (Bruzzone and Prieto, 2000; Hall and Hay, 2003; Niemeyer et al., 2008); and (4) segmenting one image and then resegmenting the segments in

* Corresponding author at: 163 Xianlin Avenue, Nanjing, China.
E-mail address: xiaopf@nju.edu.cn (P. Xiao).

http://dx.doi.org/10.1016/j.rse.2017.09.022
Received 14 February 2017; Received in revised form 8 September 2017; Accepted 16 September 2017

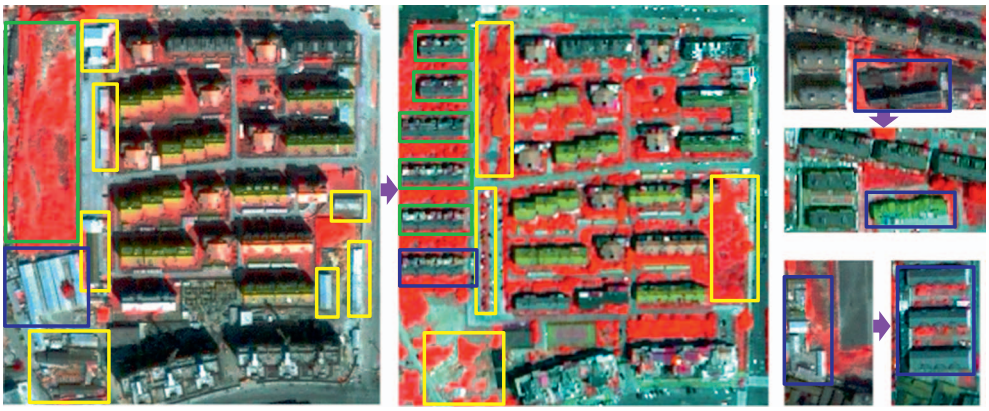

Fig. 1. Examples of changed buildings in urban area to illustrate thematic and geometric changes of geographic objects. New buildings, dismantled buildings, and restored buildings are marked as green, yellow, and blue rectangles at the corresponding positions in multi-temporal IKONOS images, respectively. The images are shown with the false-color composition of near infrared, red, and green. (For interpretation of the references to color in this figure legend, the reader is referred to the web version of this article.)

potentially changed regions for the other image (Li et al., 2009; Listner and Niemeyer, 2011). The main difference of the four segmentation solutions comes from the way of utilizing multi-temporal information. The effectiveness of them may depend on specific application tasks. Since the same unit is used for successive change analysis, it can only determine the changed regions and reveal the thematic changes in those regions. To reveal object-to-object geometric changes, the change analysis has to be performed on different units.

Providing different units for OBCD means to separately segment multi-temporal images to produce a segmentation result at each phase. The successive change analysis is then performed by comparing distinct multi-temporal segments associated with spatial correspondence. Since the segments hold the potential to represent diverse geographic objects at each phase, the geometric changes of objects can be revealed by comparing distinct segments at different phases, as shown in the blue rectangles in Fig. 2 for restored buildings. Furthermore, the separate segmentations hold a great potential of exploiting multi-temporal information for detecting thematic changes in two aspects: (1) the boundaries of changed objects can be accurately described by the separate segmentations, such as the marked changed buildings in Fig. 2; and (2) the shape change of multi-temporal segments could serve as an effective clue for determining changed objects.

Even though OBCD based on separate segmentations apparently holds theoretical advantages as described above, it faces the great challenge of establishing spatial correspondence between multi-temporal segments (Chen et al., 2012; Hussain et al., 2013; Tewkesbury et al., 2015). This is because in addition to the changed areas, the multi-temporal segments in unchanged areas also present apparent shape changes (Fig. 2), which could be caused by the contextual influence of the changed objects, the appearance change of the same geographic objects such as the material of roof and the phenology of vegetation, and the different imaging conditions such as the solar elevation, sensor angle, and atmospheric condition (Niemeyer et al., 2008). The shape changes of segments in unchanged areas make it difficult to distinguish the real shape changes from those caused by other factors rather than object changes. More importantly, a segment at one phase may overlap with multiple segments at the other phase, making it difficult to determine the spatially corresponded segments at different phases purely according to the geometric cues of segments, e.g. position, size, and shape.

Since the distinct segments in unchanged areas are the main disturbance to establishing spatial correspondence between separate segmentations, we need additional supports apart from geometric cues to suppress segments in unchanged areas and to highlight segments in changed areas. It should become relatively simple to establish spatial correspondence between distinct segments in only changed areas without the disturbance of those segments in unchanged area. Usually, the class labels of multi-temporal segments serve as an additional support. For example, we can first detect the objects of interest at each phase and then restrain to compare the detected objects for change analysis (Gong et al., 2008; Miller et al., 2005). In this case, it can naturally achieve object-to-object comparison by overlapping detected objects. However, the effectiveness is highly dependent on the object detection performance. Another possible solution is to first classify all the segments at each phase and then find changed objects with different class labels (Chen et al., 2013; Dingle Robertson and King, 2011; Gamanya et al., 2009; Lizarazo, 2012). However, at present, most studies still choose to determine changed objects on the intersections of classified objects (Dingle Robertson and King, 2011; Gamanya et al., 2009; Lizarazo, 2012). The intersection makes it degrade into change

Fig. 2. Example of separate segmentations to illustrate its advantages of revealing geometric changes (such as the restored buildings in blue rectangles) and its difficulty of establishing spatial correspondence between distinct segments at different phases. (For interpretation of the references to color in this figure legend, the reader is referred to the web version of this article.)

detection based on the same unit, and further introduces the problem of 'sliver' objects (Linke et al., 2009; McDermid et al., 2008). Even though the class labels could be helpful, how to establish spatial correspondence between multi-temporal classified objects to reveal geometric changes remains an unsolved problem.

In our previous study, we have proposed a separate segmentation method named as cosegmentation to achieve object-to-object change detection (Xiao et al., 2017). This study is an extension and generalization of cosegmentation. The contributions of this study include three aspects as followed.

1) Providing a generalized framework to achieve object-to-object change detection in urban areas based on separate segmentations. Cosegmentation is a foreground-background segmentation method. But is it necessary to exploit foreground-background segmentation method to achieve object-to-object change detection? The core idea of the framework is to first produce multi-temporal changed objects and then to perform the key step of establishing spatial correspondence on these changed objects rather than on multi-temporal image objects. In the framework, cosegmentation serves as one of the solutions to provide multi-temporal changed object. As an example, three separate segmentation strategies, including cosegmentation, are presented, showing that once the same change feature is used to produce multi-temporal changed objects, the spatial correspondence would be naturally imbedded and easy to be established by overlapping analysis.
2) Understanding the importance of associating the separate segmentation procedures for successive establishment of spatial correspondence. Usually, the separate segmentation procedures are independently performed, during which the segments in changed areas are influenced by those in unchanged areas because of the contextual effects. Is it better to associate the separate segmentation procedures to reduce the contextual influence from unchanged areas? To answer this question, we compare three separate segmentation strategies, the segmentation procedures of which are ranging from independent to associative. The differences of change detection accuracies and geometric changes indicate the importance of associating the separate segmentation procedures.
3) Demonstrating the benefits of establishing spatial correspondence on multi-temporal changed objects. It is proved that most of the removed non-corresponded changed objects during establishing spatial correspondence tends to be false detections, which can help to lower the false alarms. After establishing spatial correspondence, the advantages of object-to-object change detection based on separate segmentations are further explored in terms of both revealing and exploiting geometric changes of objects.

The rest of this paper is organized as follows. In Section 2, the study area and datasets are described. The general framework and technological details of OBCD based on separate segmentations are presented in Section 3. Section 4 shows the experimental results and discussions in urban area. The conclusions of this study are drawn in Section 5.

2. Study area and data

The study area is located in the Nanjing and Changzhou City of Jiangsu Province, China, as shown in Fig. 3. As part of the Yangtze River Delta Economic Zone, Nanjing and Changzhou have experienced rapid development over the past forty years since economic reform and openness policy (Xiao et al., 2014), which has led to significant changes of land uses in urban area, especially the extensive changes of buildings used for industrial and residential purposes. In addition, buildings are presented with clear boundaries and regular shapes in HR images, which are good examples to show the object-to-object geometric changes. Hence, we focus on detecting building changes in urban area to demonstrate the effectiveness of the proposed OBCD method on revealing geometric changes.

A pair of aerial images with 45.5 km^2 in Changzhou and a pair of IKONOS images with 107.5 km^2 in Nanjing are used as the data. To preprocess the multi-temporal images, the polynomial function is used to perform the geometric registration with residual misregistration less than 0.5 pixels. The relative radiometric correction is applied using the pseudo invariant features (Schott et al., 1988). The spatial resolution of all the images is resampled to 1 m. The aerial images in Changzhou are acquired in 2008 and 2012 by plane and unmanned aerial vehicle (UAV), respectively, covering a development zone with serious changes of new built-up areas. In this zone, a subset image with 0.7 km × 1.6 km is used to present change detection results. The dataset is named as DS1. The IKONOS images in Nanjing are acquired in 2000 and 2009. The images cover both downtown and urban fringe area. In urban fringe area, the main changes are caused by new built-up areas. While in downtown area, there are many dismantled and rebuilt buildings appeared. A subset image with 0.9 km × 1.6 km in urban fringe area (named as DS2) and a subset image with 0.7 km × 1.5 km in downtown area (named as DS3) are presented to show change detection results.

As shown in Fig. 3, the changed buildings in DS1 and DS2 are mainly new buildings, which can be described as a single change map. We make the reference map for these two datasets by manually delineating the changed buildings, as shown in Fig. 4. The two datasets are mainly used for quantitative evaluation of the proposed OBCD method. DS3 has many rebuilt buildings with apparent object-to-object geometric changes. It is mainly used for qualitatively showing the potential of revealing geometric changes of the proposed method.

3. Methodology

3.1. General framework of OBCD based on separate segmentations

To reveal geometric changes of objects, the multi-temporal HR images should be separately segmented to provide distinct segments specific to the image at each phase. The proposed OBCD framework based on separate segmentations is described as Fig. 5. First, the change feature between two phases is calculated. At the same time, the multi-temporal images are separately segmented. Then the change feature is applied to each segmentation to determine changed objects at that phase. Since the same change feature is used for detecting changed objects at different phases, it can generate multi-temporal changed objects with spatial correspondence naturally imbedded. Optionally, the changed objects can be post-processed to improve geometric accuracy. After that, the spatial correspondence between multi-temporal changed objects is apparently established, obtaining the object-to-object pairs to show geometric changes.

3.2. Generating multi-temporal changed objects from separate segmentations

Separate segmentations of multi-temporal images are specific to each phase, so that the multi-temporal segments are distinct with each other and able to show the geometric changes of geographic objects. Intuitively, we would choose to perform the separate segmentation tasks independently, in which the segments receive the equal attention in both changed and unchanged areas. However, for change detection tasks, we would only care about the segments in changed areas rather than those in unchanged areas. To achieve this, we propose to associate the separate segmentation procedures by using the same change feature between two phases. The change feature serves as the association cue and guides the segmentation procedure to pay more attention to changed areas than to unchanged areas.

Ranging from independent to associative, three separate segmentation strategies are designed and shown in Fig. 6, including: (1) separate and independent image segmentation (SIISeg), (2) separate and

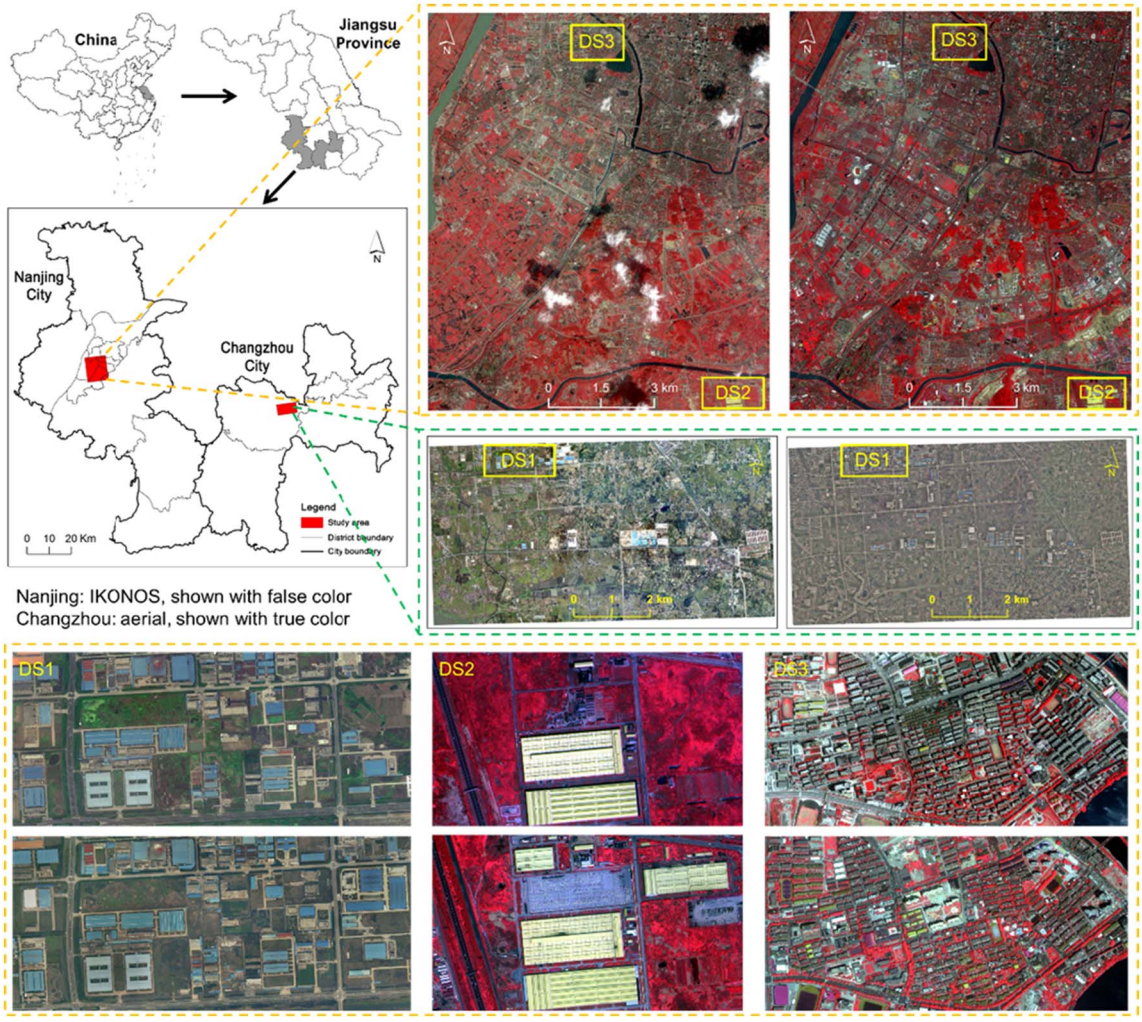

Fig. 3. Location of the study area and the datasets used to present change detection results.

associated image segmentation (SAISeg), and (3) separate and associated object segmentation (SAOSeg). We compare the three strategies to explore the effectiveness of associating separate segmentation procedures on delineating changed objects and on establishing spatial correspondence. The SIISeg and SAISeg methods provide multi-temporal segments, based on which the changed objects are successively determined by using the change feature. The SAOSeg method is a foreground-background segmentation method, based on which the changed objects are directly generated. The details of generating multi-temporal changed objects by each separate segmentation strategy are described as below.

3.2.1. Separate and independent image segmentation (SIISeg)

The segmentation procedures of SIISeg are independent at different phases. First, we separately segment the image at each phase to obtain multi-temporal segments. Concurrently, we calculate the change feature between different phases. Then, the change magnitude of each segment is calculated by averaging the change feature values over all the internal pixels. Finally, the changed objects at each phase are separately determined by thresholding the change magnitudes of the segments.

As for the segmentation method, the widely-used multi-resolution segmentation (MRS) method imbedded in the commercial software eCognition is adopted, which is a bottom-up region growing method with the key parameter of segmentation scale (Baatz and Schäpe, 2000).

The change feature (*CF*) is calculated using the change vector analysis (CVA) method for each pixel (Bovolo et al., 2012; Chen et al., 2003), as shown in Eq. (1), where V_{Tj} is the feature vector at phase T_j, n indicates the dimension of the vector. To detect changes of buildings, the feature vector is composed of spectral features and the morphological building index (MBI) (Huang et al., 2014). MBI performs an

Fig. 4. Manually delineated changed objects as reference of DS1 and DS2. There are 57 and 29 changed building objects in DS1 and DS2, respectively.

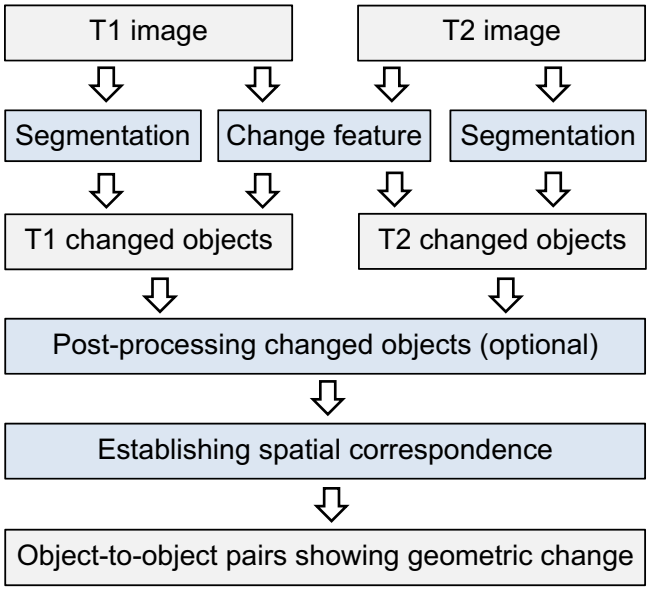

Fig. 5. Workflow of object-based change detection based on separate segmentations of multi-temporal remote sensing images (revised from Xiao et al., 2017).

effective indicator of buildings in urban area. The general idea is to build a relationship between the spectral-structural characteristics of buildings and morphological operators. According to Eq. (1), a high change feature value would indicate a great possibility to be changed building, vice versa.

$$CF = \sqrt{\sum_i (V_{T1}^i - V_{T2}^i)^2} \Big/ n \tag{1}$$

3.2.2. Separate and associated image segmentation (SAISeg)

The processing steps of producing changed objects based on SAISeg are same as those of SIISeg. However, the same change feature is separately stacked with each image at first. The segmentation step of SAISeg is performed on the stacked images rather than on the original images. Since the same change feature is involved, the separate segmentation procedures of SAISeg are not independent any more. Both segmentation procedures receive relatively high values in potentially changed areas and low values in potentially unchanged areas from the change feature. This could help to enhance the distinguishability of segments in changed and unchanged areas, but it still cannot straightly determine changed objects. The segments of SAISeg have no change labels and need to be further determined as changed or not. Hence, we observe that the change feature serves as an association cue for SAISeg at the feature level.

3.2.3. Separate and associated object segmentation (SAOSeg)

The segmentation procedure of SAOSeg at each phase is different with that of SIISeg and SAISeg. Instead of first segmenting image objects and then determining changed objects, it is a foreground-background segmentation method to directly generate changed objects. In the segmentation result, the foreground represents changed objects and the background indicates unchanged.

SAOSeg is also separately performed at each phase. The technical details of SAOSeg are referred to our previous work about co-segmentation (Xiao et al., 2017). At each phase, it is performed by minimizing an energy function composed of the same change feature and the image feature at this phase. The energy function is expressed by a graph model defined on the image, indicating the penalty of segmenting an image into foreground and background. Specifically, the energy function is defined as Eq. (2), where the term E_{change} relates to the change feature value, indicating the penalty of assigning foreground or background label to each pixel. The term E_{image} reflects the spectral difference of adjacent pixels, which helps to decide the boundaries of changed objects. λ is the weight parameter to balance the contribution of change feature and image feature. The energy function is minimized by the graph cut method (Boykov and Kolmogorov, 2004). The minimized energy function means the lowest penalty of foreground-background partition and thus produces the globally optimal segmentation result to represent changed objects at each phase.

$$E = \lambda E_{\text{change}} + (1 - \lambda) E_{\text{image}} \tag{2}$$

Since the same change feature is integrated into the energy function at each phase, the separate segmentation procedures are associated. The high change feature values guide to determine changes for both segmentation procedures. The boundaries of changed objects at each phase are jointly determined by the same change feature and the image feature at that phase. Hence, the generated multi-temporal changed objects are naturally imbedded with spatial correspondence but showing geometric change. In SAOSeg procedure, the change feature is directly involved into the determination of changed objects. Hence, we observe that the change feature serves as an association cue at the decision level for SAOSeg, compared with that at the feature level for SAISeg.

3.2.4. Post-processing

The detected changed objects could be fragmented and the boundaries may be ragged caused by the heterogeneous urban objects in HR images. In addition, several small meaningless objects would be produced because of the different imaging geometry and image noise. Accordingly, a three-step post-processing strategy is applied to the detected changed objects. The first step is a morphological closing operation to fill gaps within objects and thus to improve the completeness. The second step is a morphological opening operation to smooth the object boundaries and to eliminate the long and thin strips caused by different imaging geometries. The third step is to eliminate small patches with a size smaller than a given threshold. The parameters include

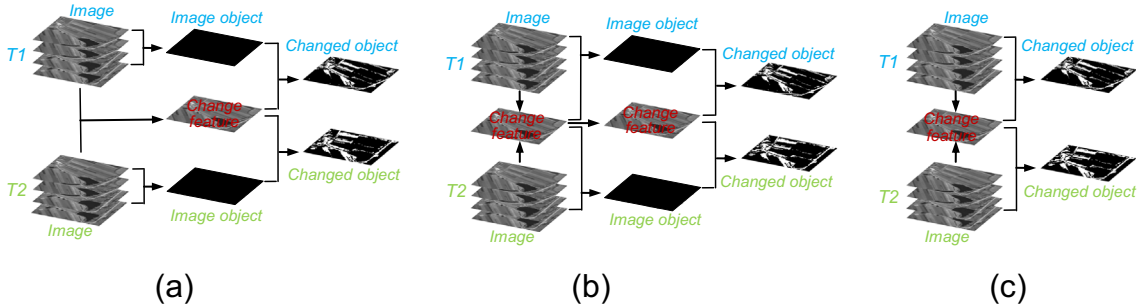

Fig. 6. Flowcharts of three separate segmentation strategies for generating multi-temporal changed objects: (a) separate and independent image segmentation (SIISeg); (b) separate and associated image segmentation (SAISeg); (c) separate and associated object segmentation (SAOSeg).

the structural element of the morphological operations and the size threshold, which should be properly set according to specific applications. In this study, the structural element is set as a square of 5 × 5 pixels, and the size threshold is set as 200 m^2.

3.3. Establishing spatial correspondence

Since the same change feature is used for producing the multi-temporal changed objects, the spatial correspondence between them is naturally imbedded. That is the changed objects at different phases should appear at the same location. The next step is to apparently establish the spatial correspondence between multi-temporal changed objects through overlapping analysis, thus revealing the object-to-object geometric changes. The spatially corresponded objects at different phases are observed having common overlapping parts.

To establish the spatial correspondence, we first overlap the two change maps composed of all changed objects at each phase. The changed objects that have no common overlapping parts at the other phase are viewed as false detections and being removed. Then the spatially corresponded objects are those having common overlapping parts. Finally, we assign the same labels to each pair of spatially corresponded changed objects. Thus the object-to-object geometric changes are revealed through the pairs of corresponded objects with the same label.

After establishing spatial correspondence, the geometric changes from former phase to later phase are clearly presented. Moreover, the geometric changes hold a potential to further verify the correctness of changed objects. We assume that a pair of changed objects with great geometric change is more confident to be real change, while that with small geometric change may tend to be fake change. To demonstrate this potential in the followed experiment section, we propose to calculate shape change index for each pair of changed objects as Eq. (3). $Obj_{T1}{}^{i}$ and $Obj_{T2}{}^{i}$ represents the ith object at the former and later phase, respectively. $|\cdot|$ is the area of a region. A great SC value indicates a large shape change. It is noted that we only try to demonstrate the potential of exploiting geometric changes for correctness verification, rather than to propose a solution for verification.

$$SC = 1 - \frac{|Obj_{T1}^{i} \cap Obj_{T2}^{i}|}{|Obj_{T1}^{i} \cup Obj_{T2}^{i}|} \tag{3}$$

4. Experimental results and discussions

4.1. Experimental setup

The experiment includes four parts. At first, the multi-temporal changed objects before and after establishing spatial correspondence are presented and evaluated to show the success and benefit of establishing spatial correspondence on changed objects. Second, the importance of associating separate segmentation procedures for establishing spatial correspondence is quantitatively demonstrated by comparing SIISeg, SAISeg, and SAOSeg. Third, the examples of revealing geometric changes by spatially corresponded changed objects are presented, and the potential of exploiting geometric changes on change correctness verification is certified. This further shows the differences among SIISeg, SAISeg, and SAOSeg about revealing geometric changes. At last, the proposed OBCD method based on separate segmentations is compared with the state-of-the-art OBCD methods based on single segmentation, aiming at showing the effectiveness of separate-segmentation-based OBCD on exploring multi-temporal information by establishing spatial correspondence.

To generate the multi-temporal changed objects, there are several parameters needed to be set, including the parameters of segmentation scale and change magnitude threshold for SIISeg and SAISeg, and the weight parameter in energy function for SAOSeg. We do not pay attention to automatically optimize these parameters but set them using the trial-and-error strategy to achieve the possible highest accuracies in terms of the *F-score* measure. Specially, the segmentation scale parameters for SIISeg and SAISeg are set the same for different phases to reduce the distinction between separate segmentations, while the other parameters are set differently for different phases to ensure high accuracies. According to the trial-and-error strategy, the segmentation scale parameters for DS1–DS3 are set as 60, 90, and 60, respectively.

To quantitatively evaluate change detection results, the measures of *precision*, *recall*, *F-score*, and *edge* are calculated by comparing with the reference shown in Fig. 4. The first three measures are defined as:

$$precision = \frac{tp}{tp + fp}, \tag{4}$$

$$recall = \frac{tp}{tp + fn}, \tag{5}$$

$$F\text{-}score = 2 \times \frac{precision \times recall}{precision + recall}, \tag{6}$$

where tp is the number of correctly detected changed pixels, fp is the number of unchanged pixels that are incorrectly detected as change, and fn is the number of changed pixels that are incorrectly detected as unchanged. A high *precision* value indicates a small number of false alarms and a high *recall* value indicates a small number of missed detections. *F-score* is evenly balanced between false alarms and missed detections, revealing the overall detection performance.

The measure *edge* reflects the accuracy of the edges of changed objects, which is calculated by first matching the detected changed object O_i to the reference object R_i (Persello and Bruzzone, 2010). For each pair of R_i and O_i, the $edge_i$ is defined as:

$$edge_i = \frac{|e(R_i) \cap e(O_i)|}{|e(R_i)|} \tag{7}$$

Specifically, an operator $e(\cdot)$ is applied to extract edge pixels of objects with a width of five pixels and the ratio between the overlapping area of the edges of (R_i, O_i) and the edge area of the reference object R_i is calculated. The *edge* value for all the matched objects are calculated as the mean of $edge_i$. A great *edge* value indicates a high edge accuracy of changed objects.

4.2. Effectiveness of establishing spatial correspondence

The first issue is to demonstrate whether the spatial correspondence can be successfully established on multi-temporal changed objects. Theoretically, since the same change feature is used by separate segmentations to generate multi-temporal changed objects, the spatial correspondences are assumed to be naturally imbedded between different phases. The multi-temporal changed objects before and after establishing spatial correspondence are presented in Figs. 7 and 8 for DS1 and DS2, respectively. We can see that the spatial correspondence between changed objects generated by SIISeg, SAISeg, and SAOSeg can all be successfully established, demonstrating the reasonability of establishing spatial correspondence on multi-temporal changed objects.

The second question is what the benefit of establishing spatial correspondence is in addition to revealing geometric change. During the establishing procedure, the non-corresponded changed objects are removed as shown in Figs. 7 and 8. Are these non-corresponded changed objects being reasonably removed? To justify this, the accuracies of multi-temporal changed objects before and after establishing correspondence are assessed and presented in Table 1. Generally, the *F-score* values are increased because the *precision* values are greatly improved while the *recall* values are slightly decreased or keeping the same after removing non-corresponded objects. This shows that most of the removed objects are false detections, causing the great increase of *precision* values, while still a few correctly detected objects are removed,

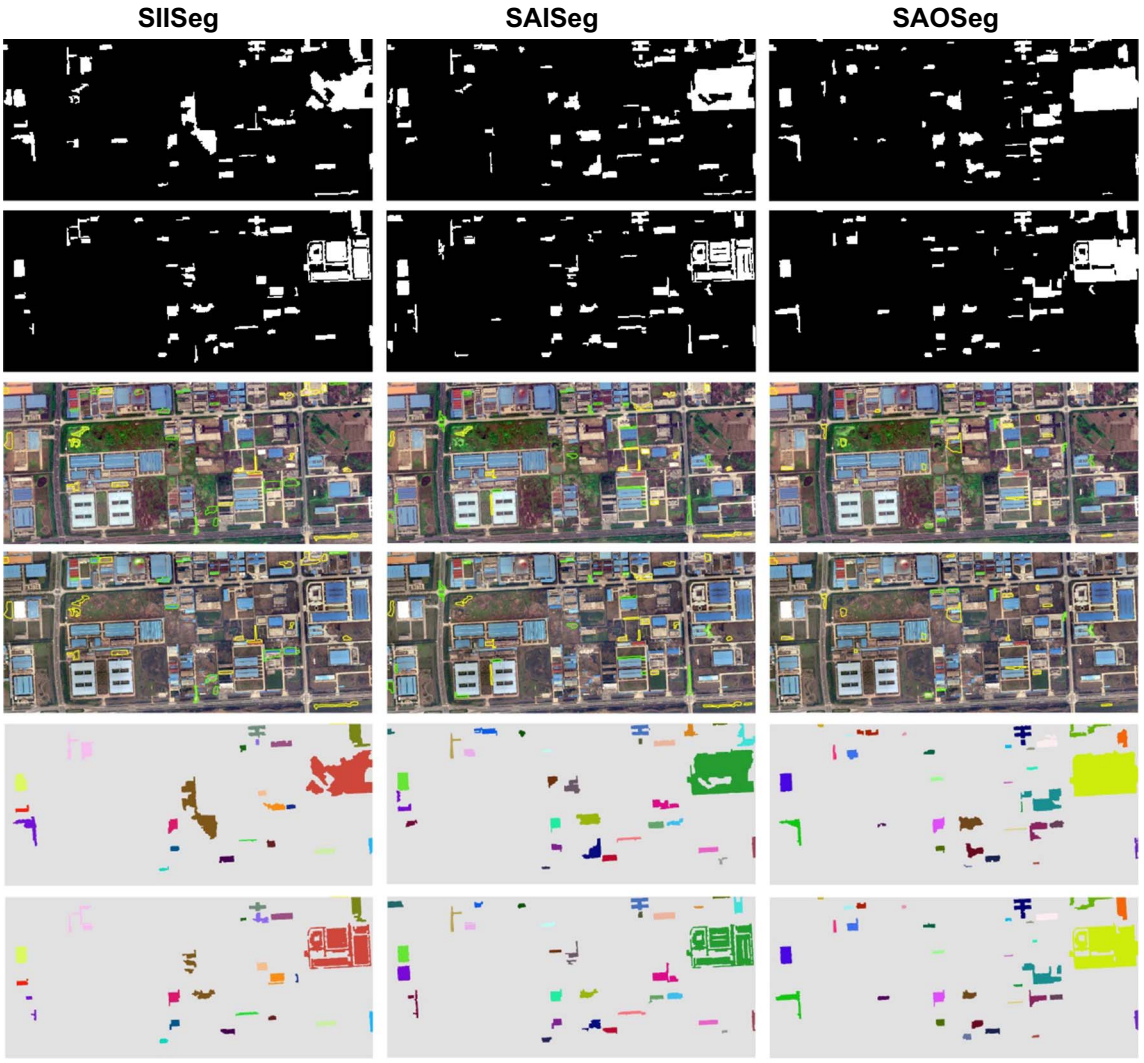

Fig. 7. Multi-temporal changed objects of DS1 before and after establishing spatial correspondence. The changed objects before establishing spatial correspondence at phase T1 and T2 are shown in the first and second rows, respectively. The removed non-corresponded changed objects are overlapped with T1 and T2 images and shown in the third and fourth rows, where the removed objects at T1 are marked as yellow and those at T2 as green. The spatially corresponded changed objects are shown in the last two rows, where each pair of corresponded objects is marked with the same color. (For interpretation of the references to color in this figure legend, the reader is referred to the web version of this article.)

leading to the slight decrease of *recall* values. Hence, one of the benefits of establishing spatial correspondence could be improving change detection accuracy by removing non-corresponded false changed objects.

The third question is then raised to explore why these non-corresponded changed objects are produced. This helps to further support the above discovery that most non-corresponded objects are false detections. Since the same changed feature is used for detecting multi-temporal changed objects, it should be caused by the distinct segments resulted from different local contexts at different phases. Taking the segmentation results of SIISeg as examples, the different segments that result in non-corresponded changed objects are zoomed in and presented in Fig. 9. In Fig. 9(a), a new building appears at phase T2. The segment at T2 accurately delineates the new building and is thus detected as changed object because of the great change magnitude. The segment at T1 describes the background. Since most of the background is not changed, the change magnitude of this segment is relatively small. The segment at T1 is thus detected as non-change, resulting in the non-corresponded changed object at T2. This non-corresponded changed object is a real change and should be avoided. Fortunately, it is avoided in both SAISeg and SAOSeg cases because the associated separate segmentation procedures can produce less distinct segments than SIISeg. In Fig. 9(b), the segment at phase T1 wrongly merges the surrounded regions because of the low contrast, while the segment at phase T2 correctly describes the boundary of this roof. As a result, the segment at T1 is detected as changed object while that at T2 is not, producing a non-corresponded changed object at T1. For this object, both SAISeg and SAOSeg also detect it as non-corresponded changed object, indicating that the segmentation methods can be further improved to overcome incorrect segmentation problem caused by low contrast. However, even though the incorrect segmentation leads to an incorrect changed object at T1, it is not spatially corresponded with an object at the other phase and is thus removed, which shows the benefit of establishing spatial correspondence to eliminate incorrect detections caused by the low image quality at one phase.

4.3. Quantitative differences caused by independently and associatively separate segmentations

As described in Subsection 3.2, the separate segmentation procedures of SIISeg are totally independent, while the segmentation procedures of SAISeg and SAOSeg are associated by the change feature at the feature and decision level, respectively. From independent to association at feature level, and even to association at decision level, we can observe the association between separate segmentation procedures

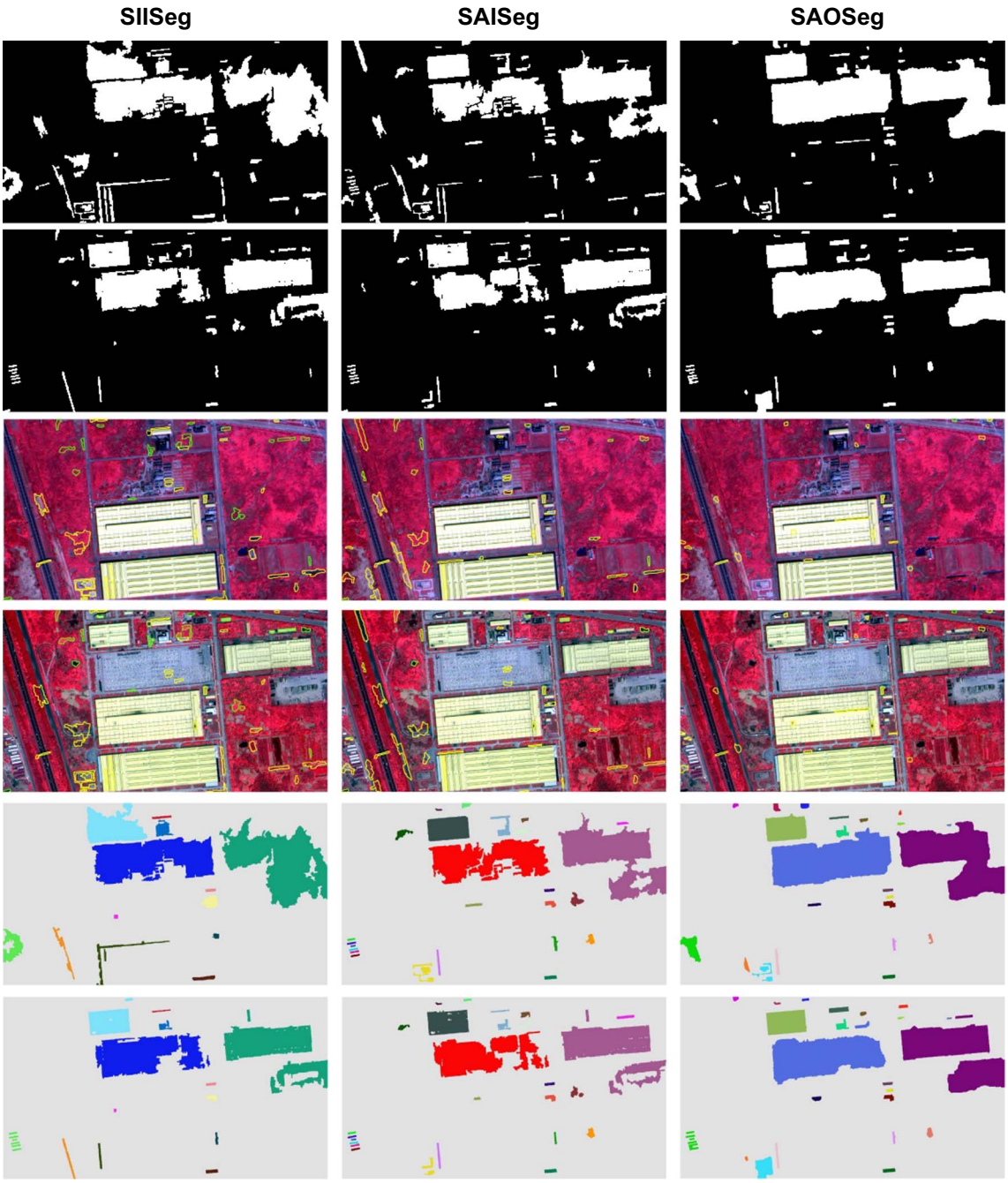

Fig. 8. Multi-temporal changed objects of DS2 before and after establishing spatial correspondence. The results are presented in the same way as those in Fig. 7.

Table 1
The accuracies of multi-temporal changed objects before and after establishing spatial correspondence.

Dataset	Phase	Corresponding	SIISeg			SAISeg			SAOSeg		
			Precision	*Recall*	*F-score*	*Precision*	*Recall*	*F-score*	*Precision*	*Recall*	*F-score*
DS1	T1	Before	0.58	0.63	0.60	0.67	0.75	0.71	0.70	0.88	0.78
		After	0.67	0.61	0.64	0.72	0.73	0.73	0.77	0.88	0.82
	T2	Before	0.80	0.73	0.76	0.73	0.71	0.72	0.86	0.90	0.88
		After	0.83	0.66	0.74	0.80	0.70	0.75	0.88	0.89	0.88
DS2	T1	Before	0.69	0.86	0.76	0.78	0.80	0.79	0.84	0.94	0.89
		After	0.76	0.85	0.80	0.88	0.79	0.83	0.86	0.94	0.90
	T2	Before	0.92	0.75	0.83	0.92	0.70	0.80	0.92	0.88	0.90
		After	0.97	0.74	0.84	0.94	0.70	0.80	0.92	0.88	0.90
Mean change of accuracies			0.06	− 0.03	0.02	0.06	− 0.01	0.02	0.03	0.00	0.01

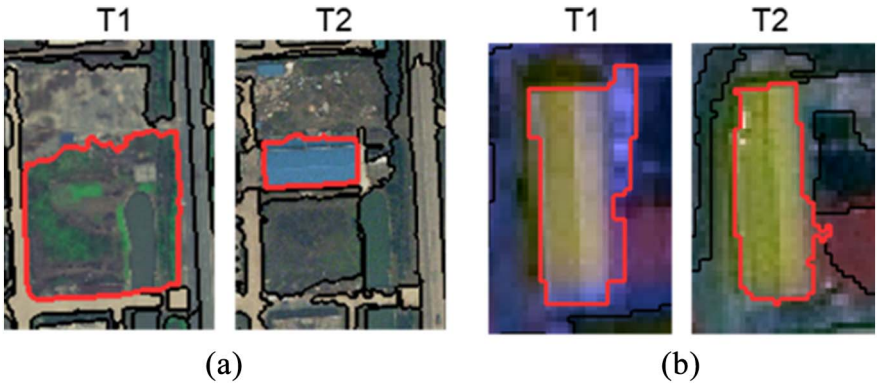

Fig. 9. Examples of non-corresponded changed objects caused by distinct segments at different phases, (a): only the segment marked as red at phase T2 is detected as changed object, (b): only the segment marked as red at phase T1 is detected as changed object. (For interpretation of the references to color in this figure legend, the reader is referred to the web version of this article.)

is getting stronger. This leads to the different performances in terms of both spatial correspondence establishment and change detection accuracies. The multi-temporal changed objects from these three segmentation methods are presented in Figs. 7 and 8 to show the visual differences. The quantitative differences are analyzed in this subsection to show the necessity of associating separate segmentation procedures for object-to-object change detection.

In terms of spatial correspondence establishment, the removed non-corresponded changed objects would lead to accuracy change. As shown in Table 1, the mean accuracy changes tend to decrease from SIISeg, SAISeg, to SAOSeg as the association is getting stronger. This is because the separate segmentation procedures would pay more attention to potentially changed areas as associated by the change feature, and the contextual influence from unchanged areas is thus suppressed. In this way, multi-temporal changed objects become less distinct, resulting in fewer non-corresponded objects as Fig. 9(a) and smaller accuracy changes. To justify the reasonability of the above explanation, we evaluate the distinctness between multi-temporal changed objects through the measure of overlay ratio (*OR*), which is the area ratio of the intersections to the unions of two change maps composed of changed objects at each phase. A large *OR* value indicates a small distinctness according to the definition. As shown in Table 2, the *OR* values are increased from SIISeg, SAISeg, to SAOSeg, which demonstrates the decrease of distinctness between multi-temporal changed objects. Accordingly, the number of removed non-corresponded objects (*NRO*) and pixels (*NRP*) tends to decrease, resulting in the decreased accuracy changes in Table 1. Specially, the decrease of *recall* changes in Table 1 means that fewer real changed objects are removed as non-corresponded changed objects. This shows the benefit of associating separate segmentation procedures on reducing the risk of producing real changed objects as non-corresponded changed objects.

In terms of the accuracies of multi-temporal changed objects, the differences caused by different association strengths among SIISeg, SAISeg, and SAOSeg are also presented in Table 1. It is first observed that since most of the changed objects are new buildings in both DS1 and DS2, the accuracies for SIISeg at phase T1 are apparently lower than those at T2. This is because the independent segmentation at T1 cannot delineate the exact boundaries of changed buildings appeared at T2 without association. However, comparing SAISeg with SIISeg, the accuracies for SAISeg at phase T1 are almost the same as those at T2, which are apparently greater than the accuracies for SIISeg at T1. This shows the effectiveness of the feature-level association on delineating the exact changed objects appeared at the other phase. The accuracies at T2 between SIISeg and SAISeg are similar, which shows that the feature-level association cannot improve the delineation of changes at the phase when they appear. Comparing SAISeg with SAOSeg, since the association is transformed from feature level to decision level, the separate segmentation procedures of SAISeg are only associated to produce segments without change label, while those of SAOSeg are associated to produce foreground segments as changed objects. The stronger association of SAOSeg leads to higher accuracies in Table 1 than those for SAISeg.

Hence, as a whole, the association from SIISeg, SAISeg, to SAOSeg is getting stronger. It results in less distinct multi-temporal changed objects and thus fewer non-corresponded changed objects, especially fewer non-corresponded real changed objects being removed during establishing spatial correspondence. It also leads to different change detection accuracies. Specially, the strongest association of SAOSeg can help to achieve the highest accuracy among these three separate segmentation strategies.

4.4. Examples of revealing and exploiting geometric changes

As shown in Figs. 7 and 8, the geometric changes of each pair of spatially corresponded multi-temporal changed objects are clearly presented, which is because the separate segmentation procedures exploit the image features specific to each phase. Three subsets from DS1–DS3 are zoomed in and shown in Fig. 10 to present the geometric changes in detail. The change types one-to-one, one-to-several, and several-to-several are presented in the DS1, DS2, and DS3 subsets, respectively. Except for the special case that the SAISeg result transforms the one-to-several change into several one-to-one changes, all the proposed separate segmentation strategies of SIISeg, SAISeg, and SAOSeg are able to reveal the different types of geometric changes. Owing to the higher change detection accuracies, we can see that the SAOSeg results can describe the changed objects both before and after the change happens better than SIISeg and SAISeg from Fig. 10.

Since the distinctness between multi-temporal changed objects is

Table 2
The overlay ratio (*OR*) of the multi-temporal changed objects, the number of removed objects (*NRO*), and the number of removed pixels (*NRP*) by establishing spatial correspondence.

Dataset	Phase	SIISeg			SAISeg			SAOSeg		
		OR	*NRO*	*NRP*	*OR*	*NRO*	*NRP*	*OR*	*NRO*	*NRP*
DS1	T1	0.56	17	16,036	0.60	19	10,171	0.77	16	10,026
	T2		13	11,014		16	9492		8	3779
DS2	T1	0.60	32	32,579	0.74	28	30,634	0.82	18	8732
	T2		18	11,805		10	5084		1	272

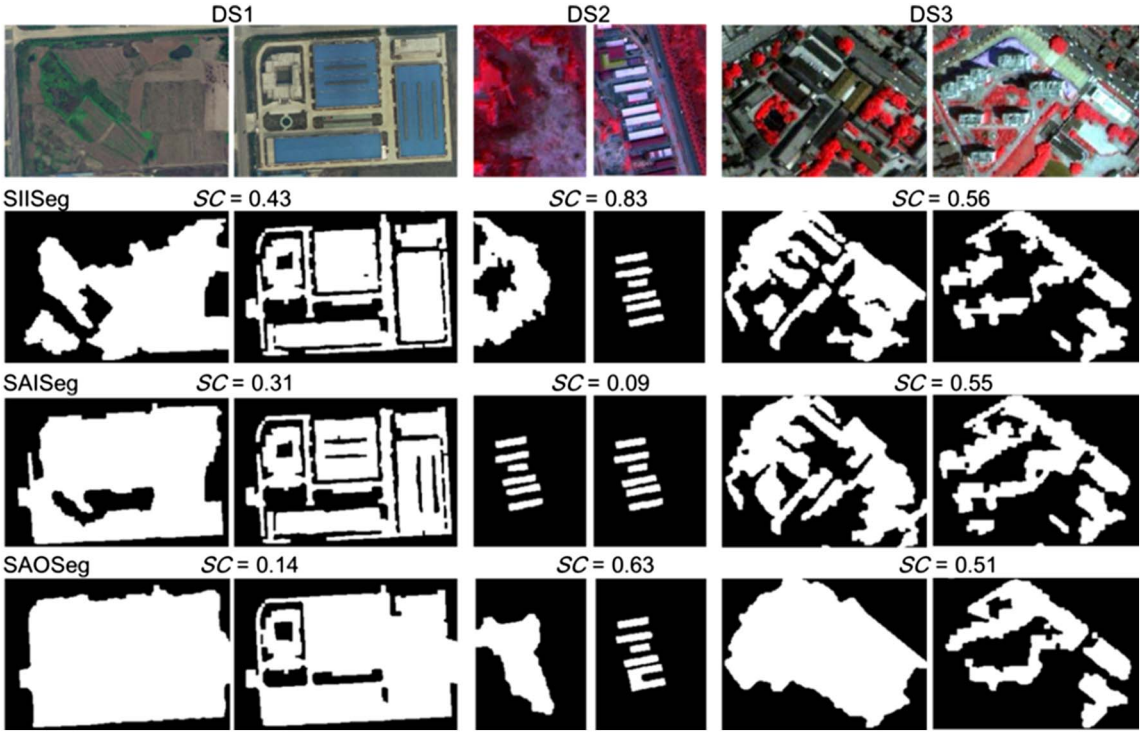

Fig. 10. Examples of corresponded multi-temporal changed objects revealing geometric changes.

Table 3
The mean shape change (*SC*) of all the changed objects and the correct changed objects.

Dataset	Mean *SC* of all the objects			Mean *SC* of correct objects		
	SIISeg	SAISeg	SAOSeg	SIISeg	SAISeg	SAOSeg
DS1	0.51	0.47	0.39	0.54	0.43	0.36
DS2	0.58	0.28	0.37	0.64	0.24	0.31
DS3	0.58	0.47	0.37			

decreased from SIISeg, SAISeg, to SAOSeg as shown in Subsection 4.3, does it mean that the changed objects at different phases tend to be similar and the geometric changes become smaller? To answer this question, we quantify the shape change (*SC*) from the former to the later phase for each pair of corresponded changed objects. Specifically, we calculate the mean *SC* of all the pairs of changed objects for SIISeg, SAISeg, and SAOSeg and show the results in Table 3. Generally, the *SC* value tends to decrease from SIISeg, SAISeg, to SAOSeg. The different *SC* values are caused by the different association strengths among the separate segmentation strategies. However, we cannot say that the greater *SC* value of SIISeg means that it can better reveal geometric changes than SAISeg and SAOSeg. This is because the geometric change of SIISeg could come from the contextual influence of unchanged areas in addition to the real change. Actually, as the association is getting stronger, the geometric changes of multi-temporal changed objects tend to be smaller. To which extent the association strength is the best for revealing geometric changes remains a problem to be discussed in the future.

To further validate the potential of utilizing the geometric change for correctness verification of changed objects, the preliminary assumption is that the real changes have relatively large geometric change, while the false changes have small geometric change. We calculate the mean *SC* values of only the correct changed objects for DS1 and DS2 and show the results in Table 3. The mean *SC* value of the correct changed objects for SIISeg is higher than that of all the objects, which means that the SIISeg changed objects with small shape change tend to be incorrect detections. An example of this case is shown in

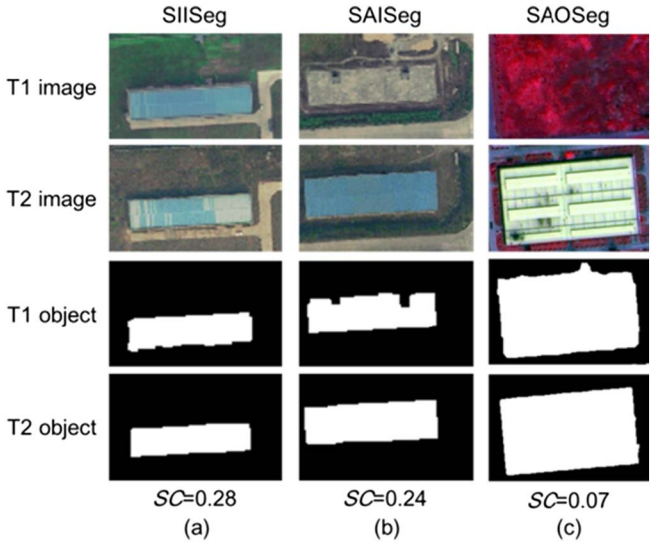

Fig. 11. Examples of corresponded multi-temporal changed objects with small shape change, (a): false change, (b) and (c): real change.

Fig. 11(a), where the material change of the roof leads to the false changed objects with small shape change. However, the mean *SC* values of the correct changed objects for SAISeg and SAOSeg are smaller than those of all the objects. This shows that the SAISeg and SAOSeg changed objects with small shape change could still be real changes, which is because the association effect in the segmentation procedures results in the changed objects with similar shape. The examples in Fig. 11(b) and (c) respectively show the SAISeg and SAOSeg results on revealing real changes of a new building but with small shape change.

As a whole, through the quantitative results of shape changes, we can find that as the association is getting stronger from SIISeg, SAISeg, to SAOSeg, the geometric changes of multi-temporal changed objects tend to decrease. We observe that the geometric change holds the potential to be an effective cue to verify changed objects especially for

SIISeg, as the corresponded changed objects with small shape change tend to have lower confidence to be real changes. But it may not be reasonable to perform the verification by simply thresholding the *SC* values. How to exploiting geometric changes for effectively verifying changed objects remains an interesting work in the future.

4.5. Comparison with single-segmentation based change detection

In this subsection, the proposed OBCD method based on separate segmentations is compared with that based on single segmentation in terms of change detection accuracy. Two single-segmentation based change detection methods are adopted for comparison. One is the Multi-Temporal Segmentation (MTSeg) method, which is to stack the multi-temporal images into an image and then to segment the stacked image (Desclée et al., 2006). The other is the Separate Segmentation Intersection (SSegInt) method, which is to separately segment the multi-temporal images at first, but the segments are then fused into a single segmentation result using the spatial intersection operation (Bruzzone and Prieto, 2000). The segmentation method and parameters of MTSeg and SSegInt are same as those of SIISeg and SAISeg for each dataset. Successively, the same CVA method is applied to the segments of MTSeg and SSegInt to detect changed objects. The change thresholds of MTSeg and SSegInt are also determined using the trial-and-error strategy to achieve the possible highest accuracies.

Specially, for this comparison, we propose to fuse multi-temporal changed objects into a single change map, which represents the upper limit on describing changes as a single map from the separate segmentations. The fusion needs the support from the reference objects. Specifically, for each pair of changed objects, the object at the phase where it can achieve higher *F-score* than that at the other phase is selected and put into the fused change map. The results of fused change map of SIISeg, SAISeg, and SAOSeg, and the results of MTSeg and SSegInt are presented in Fig. 12 for visual comparison. The accuracies of *precision*, *recall*, *F-score*, and *edge* for the results in Fig. 12 are calculated and shown in Table 4 for quantitative comparison. In addition, since the main changes are new buildings in DS1 and DS2, the changed objects at phase T2 from SIISeg, SAISeg, and SAISeg shown in Figs. 7, 8, and Table 1 are also compared with those from single segmentation.

Comparing SIISeg and SAISeg with MTSeg and SSegInt, since the segmentation and change analysis methods are the same, the main difference is that SIISeg and SAISeg produce multiple segmentations for further spatial correspondence establishment, in which non-corresponded changed objects are removed. This leads to the different change detection accuracies. Consequently, in Tables 1 and 4, we can see that the *recall* values are not greatly different, while the *precision* values of SIISeg and SAISeg results are apparently higher than those of MTSeg and SSegInt, which further proves that most of the removed non-corresponded objects are incorrect changed objects as analyzed in Subsection 4.2. The results in Fig. 12 also demonstrate this difference. That is the SIISeg and SAISeg results appear to have fewer changed objects than the MTSeg and SSegInt results, which results in higher *precision* values and thus higher *F-score* values. The *edge* values among the results produced by the four methods are not significantly different because the same MRS segmentation method is adopted. Among these five methods, the SAOSeg method achieves the best performance in terms of all the four accuracy measures, which further demonstrates the superiority of associating separate segmentation procedures at the decision level in terms of change detection accuracy.

By comparing the accuracies of SIISeg, SAISeg, and SAOSeg before fusion in Table 1 with those after fusion in Table 4, we can see the improvement of the accuracies, e.g., the improvement of *F-score* could achieve 0.05. This shows the potential of fusing multi-temporal changed objects into a single change map to further improve change detection accuracy, which could be another benefit of separate segmentations for OBCD compared with single segmentation in addition to revealing geometric change. It is noted that the reference changed objects are used to fuse the multi-temporal changed objects in this study. The fusion procedure is thus far away from automation and needs future work to solve it. To accomplish automatic fusion, we suggest to recognize the land cover type of the changed objects at first and then to determine the specific fusion strategy accordingly.

5. Conclusions

We provided a general OBCD framework based on separate segmentations of multi-temporal HR images to reveal object-to-object geometric changes, as a generalization of our previous study (Xiao et al., 2017). The core idea is to establish spatial correspondence on multi-temporal changed objects rather than on the segmented image objects, which makes it easy to perform the establishment work. The experimental results of HR images in urban areas of China, demonstrate the effectiveness of the proposed strategy.

The spatial correspondence is demonstrated to be successfully established on changed objects using a simple overlapping analysis method. In addition to revealing geometric changes, establishing spatial correspondence can help to improve change detection accuracies by removing non-corresponded changed objects. We proved that most of the removed non-corresponded changed objects are incorrect detections, which results in a higher *precision* value and thus a higher *F-score* value. This shows the benefit of separate segmentations on improving change detection accuracy compared with single segmentation.

To show the importance of associating separate segmentation procedures, we compared three separate segmentation strategies SIISeg, SAISeg, and SAOSeg ranging from independent, associated at feature level, to associated at decision level. As the association is getting stronger, the multi-temporal changed objects become less distinct, resulting in fewer non-corresponded objects to be removed during establishing spatial correspondence and thus lower risk of removing correct objects as non-corresponded objects. Among the three methods, SAOSeg can achieve the best change detection accuracy, showing the superiority of association at decision level. Moreover, the stronger association also leads to a smaller geometric change between corresponded changed objects. To which degree the association strength should be to best express geometric changes remains a problem to be discussed in the future.

Two potentials are also discovered for OBCD based on separate segmentations. One potential is to exploit geometric change to verify the correctness of multi-temporal changed objects, especially for SIISeg results, where the changed objects with small shape change tend to be false detections. However, the geometric change could not be solely used for verification. How to effectively use it for verification remains a future work. The other potential is to fuse multi-temporal changed objects into a single change map to further improve change detection accuracy. This further indicates the advantage of OBCD based on separate segmentations on exploiting multi-temporal information compared with OBCD based on single segmentation. However, how to automatically fuse multi-temporal changed objects remains to be solved in the future.

One limitation of this study is about the atmospheric correction, which is an important impactor for unsupervised change detections. We adopt the relative radiometric correction method rather than absolute correction because: (1) we do not exactly know the atmospheric parameters on the imaging date; and (2) we even do not know the calibration coefficients of the camera for the aerial dataset. It would be interesting to understand the influence of atmospheric correction especially for unsupervised change detections from HR images.

Acknowledgement

This work was supported by the National Natural Science Foundation of China (Grant No. 41601366), the National Science and Technology Major Project of China (Grant No. 21-Y20A06-9001-17/

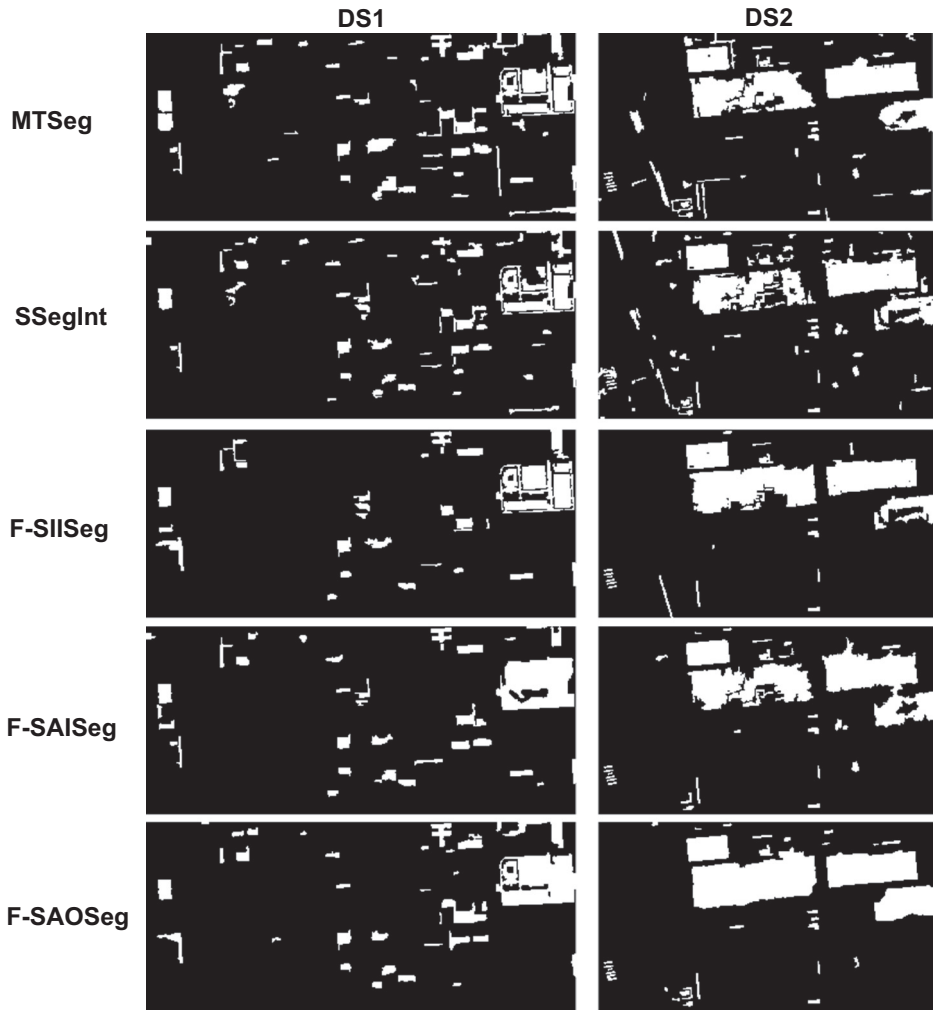

Fig. 12. Comparison of the fused change maps of SIISeg, SAISeg, and SAOSeg with the results of single-segmentation based change detection.

Table 4
Accuracy comparison of fused change maps F-SIISeg, F-SAISeg, and F-SAOSeg from multi-temporal changed objects with change maps from single-segmentation based change detection.

Method	DS1				DS2			
	Precision	*Recall*	*F-score*	*Edge*	*Precision*	*Recall*	*F-score*	*Edge*
MTSeg	0.68	0.77	0.72	0.69	0.85	0.80	0.82	0.80
SSegInt	0.77	0.70	0.73	0.69	0.81	0.73	0.77	0.78
F-SIISeg	0.84	0.68	0.75	0.75	0.95	0.80	0.87	0.77
F-SAISeg	0.81	0.77	0.79	0.73	0.91	0.79	0.85	0.83
F-SAOSeg	0.89	0.89	0.89	0.77	0.93	0.94	0.94	0.86

18), the Natural Science Foundation of Jiangsu Province (Grant No. BK20160623), and the Fundamental Research Funds for the Central Universities (Grant Nos. 020914380023, 020914380040). The authors would like to thank the anonymous reviewers and editors for their constructive comments to improve the paper.

References

Baatz, M., Schäpe, A., 2000. Multiresolution segmentation: an optimization approach for high quality multi-scale image segmentation. In: Strobl, T., Blaschke, T., Griesebner, G. (Eds.), Angewandte Geographische Informations-Verarbeitung XII. Wichmann Verlag, Karlsruhe, Germany, pp. 12–23.

Blaschke, T., 2005. Towards a framework for change detection based on image objects. Göttinger Geographische Abhandlungen 113, 1–9.

Blaschke, T., Hay, G.J., Kelly, M., Lang, S., Hofmann, P., Addink, E., Feitosa, R.Q., van der Meer, F., van der Werff, H., van Coillie, F., Tiede, D., 2014. Geographic object-based image analysis—towards a new paradigm. ISPRS J. Photogramm. Remote Sens. 87, 180–191.

Bontemps, S., Bogaert, P., Titeux, N., Defourny, P., 2008. An object-based change detection method accounting for temporal dependences in time series with medium to coarse spatial resolution. Remote Sens. Environ. 112 (6), 3181–3191.

Bontemps, S., Langer, A., Defourny, P., 2012. Monitoring forest changes in Borneo on a yearly basis by an object-based change detection algorithm using SPOT-VEGETATION time series. Int. J. Remote Sens. 33 (15), 4673–4699.

Bovolo, F., Marchesi, S., Bruzzone, L., 2012. A framework for automatic and unsupervised detection of multiple changes in multitemporal images. IEEE Trans. Geosci. Remote Sens. 50 (6), 2196–2212.

Boykov, Y., Kolmogorov, V., 2004. An experimental comparison of min-cut/max-flow algorithms for energy minimization in vision. IEEE Trans. Pattern Anal. Mach. Intell. 26 (9), 1124–1137.

Bruzzone, L., Prieto, D.F., 2000. An adaptive parcel-based technique for unsupervised change detection. Int. J. Remote Sens. 21 (4), 817–822.

Chen, J., Gong, P., He, C., Pu, R., Shi, P., 2003. Land-use/land-cover change detection using improved change-vector analysis. Photogramm. Eng. Remote Sens. 69 (4), 369–379.

Chen, G., Hay, G.J., Carvalho, L.M.T., Wulder, M.A., 2012. Object-based change detection. Int. J. Remote Sens. 33 (14), 4434–4457.

Chen, J., Mao, Z., Philpot, B., Li, J., Pan, D., 2013. Detecting changes in high-resolution satellite coastal imagery using an image object detection approach. Int. J. Remote Sens. 34 (7), 2454–2469.

Chen, G., Zhao, K., Powers, R., 2014. Assessment of the image misregistration effects on object-based change detection. ISPRS J. Photogramm. Remote Sens. 87, 19–27.

Comber, A., Law, A.N.R., Lishman, J.R., 2004. Application of knowledge for automated land cover change monitoring. Int. J. Remote Sens. 25 (16), 3177–3192.

Conchedda, G., Durieux, L., Mayaux, P., 2008. An object-based method for mapping and change analysis in mangrove ecosystems. ISPRS J. Photogramm. Remote Sens. 63 (5), 578–589.

Desclée, B., Bogaert, P., Defourny, P., 2006. Forest change detection by statistical object-based method. Remote Sens. Environ. 102 (1–2), 1–11.

Dingle Robertson, L., King, D., 2011. Comparison of pixel- and object-based classification in land cover change mapping. Int. J. Remote Sens. 32 (6), 1505–1529.

Duveiller, G., Defourny, P., Desclée, B., Mayaux, P., 2008. Deforestation in Central Africa:

estimates at regional, national and landscape levels by advanced processing of systematically-distributed Landsat extracts. Remote Sens. Environ. 112 (5), 1969–1981.
Gamanya, R., De Maeyer, P., De Dapper, M., 2009. Object-oriented change detection for the city of Harare, Zimbabwe. Expert Syst. Appl. 36 (1), 571–588.
Gong, J., Sui, H., Sun, K., Ma, G., Liu, J., 2008. Object-level change detection based on full-scale image segmentation and its application to Wenchuan earthquake. Sci. China, Ser. E: Technol. Sci. 51 (2), 110–122.
Hall, O., Hay, G.J., 2003. A multiscale object-specific approach to digital change detection. Int. J. Appl. Earth Obs. Geoinf. 4 (4), 311–327.
Huang, X., Zhang, L., Zhu, T., 2014. Building change detection from multitemporal high-resolution remotely sensed images based on a morphological building index. IEEE J. Sel. Top. Appl. Earth Obs. Remote Sens. 7 (1), 105–115.
Hussain, M., Chen, D., Cheng, A., Wei, H., Stanley, D., 2013. Change detection from remotely sensed images: from pixel-based to object-based approaches. ISPRS J. Photogramm. Remote Sens. 80, 91–106.
Im, J., Jensen, J.R., Tullis, J.A., 2008. Object-based change detection using correlation image analysis and image segmentation. Int. J. Remote Sens. 29 (2), 399–423.
Li, X., Yeh, A.G.O., Qian, J.P., Ai, B., Qi, Z., 2009. A matching algorithm for detecting land use changes using case-based reasoning. Photogramm. Eng. Remote Sens. 75 (11), 1319–1332.
Linke, J., McDermid, G.J., Laskin, D.N., McLane, A.J., Pape, A.D., Cranston, J., Franklin, S.E., 2009. A disturbance-inventory framework for flexible and reliable landscape monitoring. Photogramm. Eng. Remote Sens. 75 (8), 981–995.
Listner, C., Niemeyer, I., 2011. Object-based change detection. Photogrammetrie-Fernerkundung-Geoinformation 2011 (4), 233–245.
Lizarazo, I., 2012. Quantitative land cover change analysis using fuzzy segmentation. Int. J. Appl. Earth Obs. Geoinf. 15, 16–27.
McDermid, G.J., Linke, J., Pape, A.D., Laskin, D.N., McLane, A.J., Franklin, S.E., 2008. Object-based approaches to change analysis and thematic map update: challenges and limitations. Can. J. Remote. Sens. 34 (5), 462–466.
Miller, O., Pikaz, A., Averbuch, A., 2005. Objects based change detection in a pair of gray-level images. Pattern Recogn. 38 (11), 1976–1992.
Niemeyer, I., Marpu, P.R., Nussbaum, S., 2008. Change detection using object features. In: Object-based Image Analysis. Springer, Berlin Heidelberg, pp. 185–201.
Park, N.W., Chi, K.H., 2008. Quantitative assessment of landslide susceptibility using high-resolution remote sensing data and a generalized additive model. Int. J. Remote Sens. 29 (1), 247–264.
Persello, C., Bruzzone, L., 2010. A novel protocol for accuracy assessment in classification of very high resolution images. IEEE Trans. Geosci. Remote Sens. 48 (3), 1232–1244.
Schott, J.R., Salvaggio, C., Volchok, W.J., 1988. Radiometric scene normalization using pseudoinvariant features. Remote Sens. Environ. 26 (1), 1–16.
Stow, D., Hamada, Y., Coulter, L., Anguelova, Z., 2008. Monitoring shrubland habitat changes through object-based change identification with airborne multispectral imagery. Remote Sens. Environ. 112 (3), 1051–1061.
Tewkesbury, A.P., Comber, A.J., Tate, N.J., Lamb, A., Fisher, P.F., 2015. A critical synthesis of remotely sensed optical image change detection techniques. Remote Sens. Environ. 160, 1–14.
Xiao, P., Wang, X., Feng, X., Zhang, X., Yang, Y., 2014. Detecting China's urban expansion over the past three decades using nighttime light data. IEEE J. Sel. Top. Appl. Earth Obs. Remote Sens. 7 (10), 4095–4106.
Xiao, P., Yuan, M., Zhang, X., Feng, X., Guo, Y., 2017. Cosegmentation for object-based building change detection from high-resolution remotely sensed images. IEEE Trans. Geosci. Remote Sens. 55 (3), 1587–1603.
Zhou, Z., Huang, J., Wang, J., Zhang, K., Kuang, Z., Zhong, S., Song, X., 2015. Object-oriented classification of sugarcane using time-series middle-resolution remote sensing data based on AdaBoost. PLoS One 10 (11), e0142069.